LANGMUIR Article
Cite This: Langmuir 2018, 34, 12259−12269
pubs.acs.org/Langmuir

Quantifying Confidence in DFT-Predicted Surface Pourbaix Diagrams of Transition-Metal Electrode−Electrolyte Interfaces

Olga Vinogradova,[†] Dilip Krishnamurthy,[‡] Vikram Pande,[‡] and Venkatasubramanian Viswanathan*[,†,‡]

[†]Department of Chemical Engineering and [‡]Department of Mechanical Engineering, Carnegie Mellon University, Pittsburgh, Pennsylvania 15213, United States

Supporting Information

ABSTRACT: Density functional theory (DFT) calculations have been widely used to predict the activity of catalysts based on the free energies of reaction intermediates. The incorporation of the state of the catalyst surface under the electrochemical operating conditions while constructing the free-energy diagram is crucial, without which even trends in activity predictions could be imprecisely captured. Surface Pourbaix diagrams indicate the surface state as a function of the pH and the potential. In this work, we utilize error-estimation capabilities within the Bayesian ensemble error functional with van der Waals correlations exchange correlation functional as an ensemble approach to propagate the uncertainty associated with the adsorption energetics in the construction of Pourbaix diagrams. Within this approach, surface-transition phase boundaries are no longer sharp and are therefore associated with a finite width. We determine the surface phase diagram for several transition metals under reaction conditions and electrode potentials relevant for the oxygen reduction reaction. We observe that our surface phase predictions for most predominant species are in good agreement with cyclic voltammetry experiments and prior DFT studies. We use the OH* intermediate for comparing adsorption characteristics on Pt(111), Pt(100), Pd(111), Ir(111), Rh(111), and Ru(0001) since it has been shown to have a higher prediction efficiency relative to O*, and find the trend Ru > Rh > Ir > Pt > Pd for (111) metal facets, where Ru binds OH* the strongest. We robustly predict the likely surface phase as a function of reaction conditions by associating confidence values for quantifying the confidence in predictions within the Pourbaix diagram. We define a confidence quantifying metric, using which certain experimentally observed surface phases and peak assignments can be better rationalized. The probabilistic approach enables a more accurate determination of the surface structure and can readily be incorporated in computational studies for better understanding the catalyst surface under operating conditions.

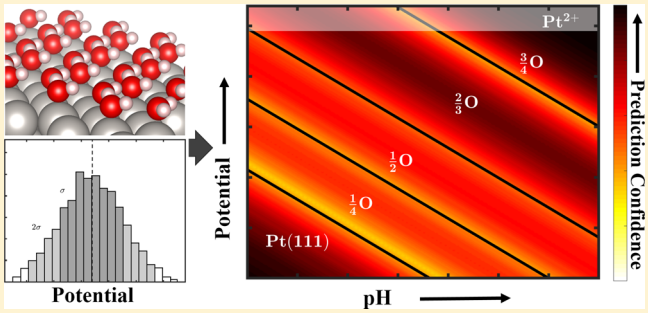

1. INTRODUCTION

Electrochemical processes are at the heart of many routes toward sustainable energy storage in the form of chemical bonds.[1] The storage routes involve hydrogen and oxygen electrochemistry occurring at solid−liquid interfaces.[2] Determining the activity of electrode materials active for these processes requires a thorough understanding of the surface dynamics at the electrode−electrolyte interfaces.[3]

Probing the electrode−electrolyte interface directly is an extremely challenging problem.[4] There has been substantial development toward the coupling of X-ray spectroscopy directly with electrochemical cells.[5,6] This can be complemented by electrochemical impedance spectroscopy to deconvolute the signals and assign them to surface-adsorbed species.[7] Theoretically, density functional theory (DFT) calculations have been used to construct surface phase diagrams based on probing many different possible surface configurations.[8] There have also been efforts to utilize both experimental and theoretical data.[9,10]

The molecular structure of the surface is crucial for determining a variety of electrochemical reactions. This is determined by the ab initio thermodynamics of key reaction intermediates. The surface Pourbaix diagram[11] depicts the most stable surface structures as a function of electrode potential U and pH under the assumption that reactions are thermodynamically constrained and has been used to understand the electrochemical landscape of reactions, such as chlorine evolution.[12,13] This has been combined with computationally derived free-energy diagram of reactions to rationalize experimental trends.[14,15] More recently, this approach has been applied for understanding Li-ion battery materials.[16,17] However, a major challenge associated with using density functional theory for predictive purposes is that the choice of the exchange correlation (XC) functional often

Received: July 2, 2018
Revised: September 12, 2018
Published: September 21, 2018

DOI: 10.1021/acs.langmuir.8b02219
Langmuir 2018, 34, 12259−12269

plays a key role in determining the dominant surface phases.[18,19]

Quantifying the error associated with calculations from density functional theory has been a critical topic of discussion for determining the intrinsic accuracy of predictions. In a previous study, Exner et al. determined error in the activity volcano for chlorine evolution from a scaling relationship between reaction intermediates on different sites, which is computationally expensive.[20] Recently, the use of Bayesian error-estimation techniques has brought capabilities to estimate uncertainty associated with DFT simulations in a more efficient manner than performing multiple individual calculations.[21] In this work, we develop a systematic method to assign a confidence value (c-value) associated with the stable surface phases at a given electrode potential and pH. Using this method, we probe the surface Pourbaix diagram of several transition metals: Pt, Pd, Ir, Rh, and Ru. We then map c-values onto the surface Pourbaix determined with the best-fit functional to gain insight into surface phase transitions and compare them with those determined by cyclic voltammetry experiments.

On the basis of our method, we identify that on Pt(111) at an electrode potential of 0.65 V (vs reversible hydrogen electrode (RHE)) the surface could be covered with a combination of OH* or O* with relatively equal confidence. Our method reproduces the well-known uncertainty associated with the DFT-predicted OH* to O* phase transition on Pt(111).[22] In determining phase transitions of interest, we model OH* and O* adsorption in fractions of a single monolayer (ML)-coveraged surface. For example on Pt(100), we consider water layer-stabilized OH* adsorption as both 1/2ML coverage of OH* (equal numbers of OH* and water adsorbed sites) and 1/3ML coverage OH* (equals numbers of OH* adsorbed, water adsorbed and empty sites). In the rest of this work, we shorthand 1/2 single ML coverage of OH* in the form of 1/2OH* for all oxygen-covered surfaces considered. On Pt(100), we note that the predicted stable phases of 1/3OH* and 1/2OH* are consistent to the suggested structural transitions by Han et al.[23] Our results indicate that on Pd(111) at potentials starting at ∼0.75 V (vs RHE), the surface is O* covered, consistent to the experimentally determined current peak corresponding to oxidation.[24] On Ir(111), Rh(111), and Ru(0001), we find voltage regimes where our prediction confidence is limited relative to other surfaces explored in this work. The order of relative adsorption strengths of 1/3OH* on (111) facet metals is Ru > Rh > Ir > Pt > Pd (in decreasing adsorption strength where Ru is most oxophilic). Except for the order between Pt and Pd, this ordering is comparable to the trend established in a previous computational study by Karlberg et al.[25] However, we observe that the adsorption strengths of 1/3OH* on (111) facets of Pt and Pd are very close to each other (within 0.02 eV) demonstrating a need to consider prediction uncertainty.

We show that we can use c-value calculation to consider a wide array of functionals within DFT to assign an error to each adsorption energy. This is particularly helpful in distinguishing between surface phases close to each other in energy. Wider distributions of c-values correspond to greater uncertainties and vice versa. Comparing the widths of c-value energy distributions with cyclic voltammetry studies, we also consider a situation where the Rh(111) surface could reconstruct into metal oxides to explain certain features in cyclic voltammograms. Given the importance of the stable state of the surface in determining electrochemical reaction mechanisms, we believe that this method will be extremely crucial in constructing free-energy diagrams on the appropriate surface and will play an important role in defining activity volcano relationships as a function of an appropriate oxygen-covered surface determined by the surface Pourbaix diagram and thus in analyzing the subsequent limiting potential.[26,27]

2. METHODS

2.1. Construction of Surface Pourbaix Diagrams. The surface Pourbaix diagram represents the stable state of the catalyst surface in electrochemical systems as a function of pH and the electrode potential U. Within this approach, the electrochemical reaction is described by a set of surfaces with adsorbed intermediates where the actual surface reaction is suppressed. Therefore, the surface Pourbaix diagram presents the thermodynamically most stable surface under fixed reaction conditions. This approach has been utilized previously[28,29] and it is well accepted that such an approach is representative of the reaction without necessitating prohibitively expensive computational resources. Consider an arbitrary metal surface S with adsorption site * in its pristine state. A generalized representation of the adsorption of oxygenated intermediates, denoted as $O_mH_n^*$, can be written as

$$S\text{-}O_mH_n^* + (2m - n)(e^- + H^+) \rightleftharpoons S^* + mH_2O \quad (1)$$

where m and n are the number of oxygen and hydrogen atoms in the adsorbate, respectively. Note that this representation corresponds to a concerted proton-coupled electron-transfer reaction. The associated free-energy change can be computed as

$$\Delta G(U, \mathrm{pH}) = G_{S^*} + mG_{H_2O} - G_{S\text{-}O_mH_n^*} - (2m - n)(G_{e^-} + G_{H^+}) \quad (2)$$

Rewriting eq 2, the free energy of electrons G_{e^-} is defined as $-eU$ where e is the electron charge. The free energy of protons G_{H^+} is determined from the computational hydrogen electrode using the equilibrium relation $H^+ + e^- \rightleftharpoons \frac{1}{2}H_2$. This gives at nonstandard conditions $G_{H^+} + G_{e^-} = \frac{1}{2}G_{H_2} - eU_{SHE} + k_BT(\ln[a_{H^+}])$ where U_{SHE} is the potential relative to the standard hydrogen electrode (SHE). We then write the free-energy change for adsorption of $O_mH_n^*$ intermediates as

$$\Delta G(U, \mathrm{pH}) = G_{S^*} + mG_{H_2O} - G_{S\text{-}O_mH_n^*} - (2m - n)\left(\frac{1}{2}G_{H_2} - U_{SHE} - 2.303k_BT\ \mathrm{pH}\right) \quad (3)$$

Therefore, we can derive a relation between potential and pH for a wide variety of adsorbates on a surface S in reference to standard conditions when $\Delta G(U, \mathrm{pH}) = 0$.

Similarly, generalized pH-independent electrochemical reactions, such as the dissolution of metal surfaces, can be represented as

$$S^{i+} \rightleftharpoons S^{j+} + (j - i)e^- \quad (4)$$

where i and j represent the charge on the ion, which can be zero for metal surfaces and uncharged species. The free energy would therefore be pH-independent and appear as a horizontal line on the surface Pourbaix, and the standard reduction potentials are taken from the CRC handbook.[30] We note that unconcerted electrochemical reactions can be represented as linear combinations of the two generalized forms presented above.

Since the most stable state at a given condition is that which minimizes free energy, we determine the surface Pourbaix diagram by choosing the appropriate state at each set of conditions of U and pH. The phase transitions between adsorbates appear as lines with a slope of −59 mV/pH ($-k_BT/e \ln 10$) and are reported as per electron transferred at standard conditions. Free energies are determined from calculated energies of adsorption E_{S^*} corrected for entropy, S, and

DOI: 10.1021/acs.langmuir.8b02219
Langmuir 2018, 34, 12259−12269

zero point energies, ZPE, which we assume do not change significantly with temperature, by $\Delta G = \Delta E_{\mathrm{ref,water}} - T\Delta S + \Delta \mathrm{ZPE}$. Values for entropy and zero point energy correction are given in the Supporting Information Section S5. In this work, we assume constant zero point energies across the ensemble of functionals for simplicity, since it is expected to have negligible variation (of order kT, where k is the Boltzmann constant) relative to the order of magnitude ($10-20kT$) of the surface energetics.

2.2. Bayesian Error-Estimation Framework. With the recent development of the Bayesian ensemble error functional with van der Waals correlations (BEEF−vdW),[21] there exists a systematic approach to estimate the uncertainty in energetics of a DFT calculation. BEEF−vdW is a semiempirical exchange correlation (XC) functional, including nonlocal contributions, developed by using training data sets for molecular formation energies, molecular reaction energies, molecular reaction barriers, noncovalent interactions, solid-state properties, and chemisorption on solid surfaces.

The exchange correlation energy in BEEF−vdW is expressed as a sum of the generalized gradient approximation (GGA) exchange energy expanded using Legendre polynomials, the local-density approximation and Perdew−Burke-Ernzerhof (PBE)[31] correlation energies and the nonlocal correlation energy from vdW-DF2.[32]

$$E_{\mathrm{XC}} = \sum_m a_m E_m^{\mathrm{GGA}\text{-}x} + \alpha_c E^{\mathrm{LDA}\text{-}c} + (1-\alpha_c)E^{\mathrm{PBE}\text{-}c} + E^{\mathrm{nl}\text{-}c} \tag{5}$$

The parameters a_m and α_c are optimized with respect to the above-mentioned data sets. The error-estimation functionality is enabled by deriving an ensemble of energies from an ensemble of exchange correlation functionals non-self-consistently following a self-consistent DFT calculation. The ensemble of exchange correlation functionals is generated using a probability distribution function for the parameters a_m and α_c, such that the standard deviation of the ensemble of energies reproduces the standard deviation for the training properties calculated using BEEF−vdW self-consistently.

2.3. Prediction Confidence of Surface Pourbaix Diagrams. Pourbaix diagrams (Figure 1) typically depict only the most stable state of the surface (minimum Gibbs free energy) over a range of operating potentials (U) and pH values with sharp phase boundaries. We utilize error-estimation capabilities within the BEEF−vdW exchange correlation functional to determine the ensemble of free energies for all considered states as a function of U and pH. Therefore, for every functional there exists a unique set of stable surface states in the ranges of pH and U of interest, determined by the corresponding minimum free-energy surface state. This results in an ensemble of Pourbaix diagrams, allowing us to apply statistical tools to obtain a measure of the confidence in a predicted surface state by quantifying the agreement between functionals. We are interested in determining the level of agreement between functionals at the GGA level as to the most energetically favorable surface state as a function of potential and pH. We use the confidence value[12,33] (c-value), which in this context is defined as the fraction of the ensemble, that is in agreement with the hypothesis of the optimal BEEF−vdW (best-fit) functional, and is given by

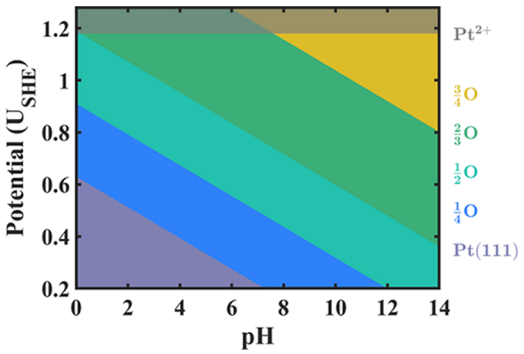

Figure 1. For Pt(111) the surface Pourbaix diagram shows regions of stability for surface coverages of OH* and O* at conditions of pH and potential relative to the standard hydrogen electrode (SHE). Dissolution of Pt is shown at 1.18 V and is independent of pH.

$$\mathrm{c}(U, \mathrm{pH}) = \frac{1}{N_{\mathrm{ens}}}\sum_{n=1}^{N_{\mathrm{ens}}} \prod_{s_i \neq s_{\mathrm{opt}}} \Theta(\Delta G_{s_i}^n(U, \mathrm{pH}) - \Delta G_{s_{\mathrm{opt}}}^n(U, \mathrm{pH})) \tag{6}$$

where N_{ens} is the number of functionals in the ensemble, which is 2000 in this work. $\Theta(x)$ denotes the Heaviside step function. At any given U and pH, $s_i \in S$, the set of all considered surface states and s_{opt} is the thermodynamically stable surface state predicted by the BEEF−vdW optimal functional. $\Delta G_{s_i}^n$ refers to the free energy of the ith surface state given by the nth member of the ensemble of functionals. This approach allows assigning confidence values to calculated surface Pourbaix diagrams.

In regimes of electrode potential and pH where the confidence value is lower than 1, it is important to determine whether the stable surface phase predicted by the majority of functionals agrees with the hypothesis of the best-fit functional. We extend the concept of c-value to determine a measure of confidence in any considered surface phase being the lowest in free energy, looking beyond just agreement with respect to the most stable phase in accordance with the optimal functional hypothesis. To define this measure, we use sp(U, pH) as the function that maps electrochemical conditions to the corresponding most stable surface phase ("sp" for "stable phase") from the set of possible/considered phases denoted by {0, 1, 2,..., i,..., n}, where i denotes the ith surface phase and $i = 0$ indicates the clean surface. For example, for the ith considered surface phase, we define below the respective stability confidence measure $\mathrm{c}_{\mathrm{sp}=1}(U, \mathrm{pH})$ quantitatively as the fraction of functionals that predict that the phase labeled as $i = 1$ is the lowest in free energy

$$\mathrm{c}_{\mathrm{sp}=i}(U, \mathrm{pH}) = \frac{1}{N_{\mathrm{ens}}}\sum_{n=1}^{N_{\mathrm{ens}}} \delta(\mathrm{sp}^n(U, \mathrm{pH}) - i) \tag{7}$$

where $\delta(x)$ denotes the Dirac delta function and the superscript n denotes the prediction from the nth functional.

3. RESULTS AND DISCUSSION

We use the example case of the surface phase diagrams relevant for oxygen reduction reaction (ORR) on Pt-group transition metals: Pt, Pd, Ir, Rh, and Ru, to demonstrate an approach to quantify the ability of DFT in determining the state surface state. We present our findings and compare them to experimental cyclic voltammetry measurements and discuss the degree of confidence in our DFT predictions in relation to the assignment of voltammetric peaks.

3.1. Pt(111). The Pourbaix diagram for Pt(111), previously investigated,[8,22] is calculated using the BEEF−vdW exchange correlation functional and is shown in Figure 1. We consider the following oxygenated adsorbate surface states of Pt(111): 1/3OH*, 1/4O*, 1/3O*, 1/2O*, 2/3O*, 3/4O*, and 1O*. While modeling OH* with water stabilization effects, we ignore potential-dependent water orientation effects,[34] and we neglect water stabilization for O* states[22,35] as both of these effects have been shown to have a negligible influence on the energetics and have yielded positive results in previous electrochemical reaction material searches in combined theory−experiment studies.[36−38] Locally mixed surface phases O*−OH* have been previously calculated[6,39] to be energetically unfavorable and are not considered since surface O* repels water unlike adsorbed OH*, where a hexagonal water stabilizing layer occurs due to favorable hydrogen bonding.[18,35] In addition, mixed phases are complex to simulate[22] since they

DOI: 10.1021/acs.langmuir.8b02219
Langmuir 2018, 34, 12259−12269

involve the incorporation of long-range disorder, which is undoubtedly present.[38] We also neglect configurational entropy of adsorbed oxygen intermediates, since the effect is expected to be small.[40]

The state of the surface is governed by the following water discharge reactions where * refers to an adsorption site on a metal catalyst surface

$$H_2O + * \rightleftharpoons OH^* + e^- + H^+$$

$$H_2O + * \rightleftharpoons O^* + 2e^- + 2H^+$$

We compute the free-energy changes of these reactions, which are functions of the pH and the electrode potential, based on eq 3 (refer Section 2.1).

$$\Delta G = \left(G_{OH^*} + \frac{1}{2}G_{H_2} - G_{H_2O}\right) + k_B T \ln[a_{H^+}] - eU \quad (8)$$

$$\Delta G = \frac{1}{2}(G_{O^*} + G_{H_2} - G_{H_2O}) + k_B T \ln[a_{H^+}] - eU \quad (9)$$

The surface Pourbaix diagram for Pt(111) shown in Figure 1 is constructed using eqs 8 and 9. The free energy as a function of the electrode potential (Figure 2) determines the surface phase

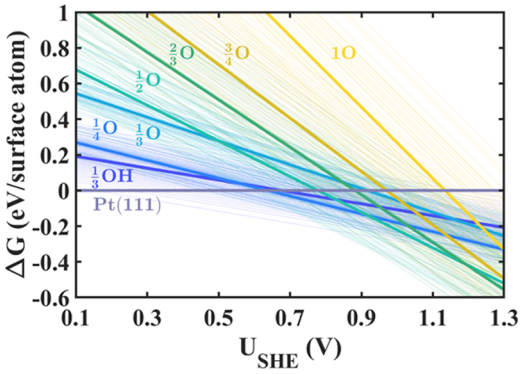

Figure 2. Comparing free energies of all coverage fraction surfaces sampled for Pt(111) at pH = 0 we observe from the best-fit solutions (thick lines) that 1/4O* is <0.05 eV more stable than 1/3OH* at 0.63 V. The thin lines represent solutions for free energy for a sample set of 50 BEEF−vdW ensemble functionals depicting a spread of energies for each surface state determined using the best-fit functional.

boundaries from the best-fit BEEF−vdW XC-functional and therefore identifies the most stable state of the surface at given reaction conditions of potential and pH. At proton activity of $a_{H^+} = 1$, we predict that below ≈0.63 V (vs RHE), clean Pt(111) surface is the most stable. Water oxidation occurs at higher potentials starting with 1/4 monolayer coverage of O* and increasing monotonically to coverage 1/2O* at ≈0.91 V (vs RHE). At 1.18 V, we indicate Pt dissociation[30] through Pt ⇌ Pt^{2+} + $2e^-$, which is pH-independent and appears as a horizontal line on the surface Pourbaix diagram. We note that this is a simplified model of Pt dissolution and likely the formation of and chemical dissolution of Pt oxide films are also important to consider, but outside the present scope of study.[41,42] Although there exist some differences in the positions of the phase boundaries, the observed set of stable surface states is consistent to those predicted by Hansen et al.[8] using the revised Perdew−Burke−Ernzerhof (RPBE) XC-functional with the exception of the 1/3OH* surface state, which Hansen et al. predicts at 0.78 V (vs RHE). However, we observe that in the range 0.63−0.83 V (vs RHE) the 1/4O* surface is marginally (by <0.05 eV) more stable than the 1/3OH* surface state, an observation also noted by Hansen et al. in the region 0.78−0.84 V. Close energetics can be resolved more robustly through the quantification of confidence in the relative stability of surface phases by the use of error-estimation capabilities based on agreement between functionals at the GGA level. Using the BEEF−vdW best-fit functional, we compute the equilibrium potential of the 1/3OH* surface state to be 0.68 V (vs RHE). Since the ensemble of functionals within the BEEF−vdW family of functionals give rise to an ensemble of energies, we quantify the uncertainty by the standard deviation of the distribution, computed to be σ_{OH} = 0.23, which bounds within the 68% confidence interval the calculation of 0.81 V by Rossmeisel et al.[22] using the RPBE XC-functional. Other examples of calculations bound within one standard deviation of the ensemble approach include the OH* adsorption energy computed by Taylor et al.[43] to be 0.59 V for a lower coverage of 1/9OH* using the PW91 XC-functional and the adsorption potential for 1/3OH* to be 0.71 V (PBE XC-functional) and 0.69 V (RPBE XC-functional) by Jinnouchi et al.[19] Similarly, calculations using RPBE XC-functional by Anderson et al. measured adsorption of a variety of combinations of OH* and H_2O fractions, observing that adsorbed OH* begins to form at ∼0.6 V.[18]

The ensemble of functionals within the BEEF−vdW XC-functional results in an ensemble of free energies for each state (Figure 2), which gives rise to an ensemble of Pourbaix diagrams.[12] Using c-value to quantify confidence in the predicted surface surface phases based on the fraction of the ensemble that is in agreement with the hypothesis of the best-fit (or optimal BEEF−vdW) functional, we construct a modified surface Pourbaix diagram following the methodology described in Section 2.3. The confidence-derived surface Pourbaix diagram of Pt(111) with the associated c-values is shown in Figure 3a. We note that regions spanning surface phase transitions are those with the lowest c-values. To better understand the relative confidence values, we show the c-values of each surface phase as a function of potential at fixed pH value of 0 in Figure 3b. We plot $c_{sp=i}$(pH, U) (refer to eq 7 of Section 2.3) for all i corresponding to the various considered surface phases to capture the degree of agreement between functionals as to the lowest free-energy phase.

The phase transitions in Figure 3b predicted by the max($c_{sp=i}(U)$) curve at fixed pH values lie within 0.02 eV of those predicted by the optimal BEEF−vdW XC-functional. We observe that the distribution of confidence values for OH* is wider than that for the O* phases and attribute this to a larger standard deviation in the distribution of energies for water-stabilized OH* (σ_{OH} = 0.23 eV) compared to O* (σ_O ≈ 0.1 eV) in reference to a water layer. The distributions of the free energies of adsorption have similar widths, however, in calculating the equilibrium potential, O* is associated to the concerted transfer of two protons and electrons, whereas the formation of OH* involves only one proton-coupled electron transfer (eqs 8 and 9). The additional factor of 2 provides rationale for the tightening of the equilibrium potential distribution for O* relative to OH*. We discuss the relative confidence values of the various phases at pH = 0, however, at different pH values the effect can be captured by a constant chemical potential shift of the proton activity (see Supporting Information Section S8). At any given potential U_{RHE}, the sum

DOI: 10.1021/acs.langmuir.8b02219
Langmuir 2018, 34, 12259−12269

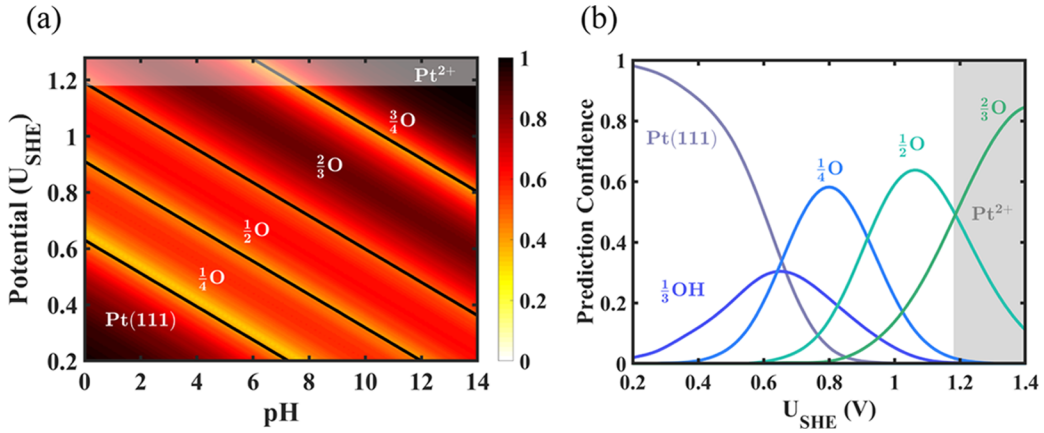

Figure 3. (a) Shows the prediction confidence of each stable surface of a Pourbaix diagram for Pt(111). Greatest prediction uncertainty occurs at phase transition boundaries. In (b) we plot the prediction confidence in relation to potential at pH of 0. Surface states with the largest c-values correspond to the solution determined with the best-fit BEEF−vdW XC-functional in Figure 1. We also note that this representation of state surfaces may be extended to higher pH values (refer to Supporting Information Section S8).

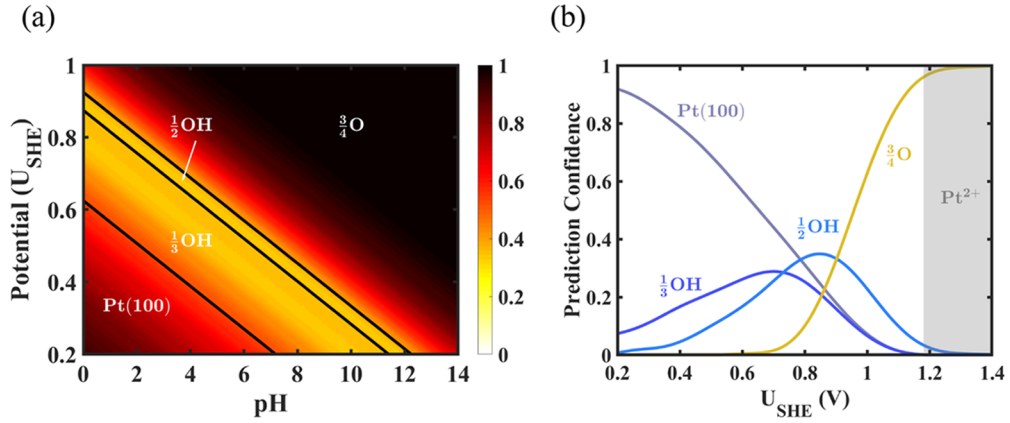

Figure 4. (a) Shows the surface Pourbaix diagram for Pt(100) where the onset of 1/3OH* is at 0.64 V (vs RHE). A free-energy vs potential figure is presented in the Supporting Information Section 9.1. (b) Depicts the c-value for each surface state at pH = 0. We observe a gradual transition from 1/3OH* to 1/2OH* from ∼0.6 to ∼0.9 V (RHE). At U_{RHE} > 0.9 V there is greatest likelihood of observing 3/4O*. The region on the *x*-axis shaded in gray represents the dissolution potential occurring at 1.18 V for Pt.

of c-value of all phases will equal to 1. Given at reaction conditions of interest, several distinct surface states are competing, and a c-value of 0.2 or above is statistically significant. At U_{RHE} < 0.55 V, we predict the clean Pt(111) surface with the highest c-value (>0.5). Around ≈0.63 V (RHE), we find that the confidence values of the clean Pt(111), 1/3OH*, and 1/4OH* are nearly equal (≈0.33) indicating that within DFT at the GGA level these surface phases are equally likely to be the lowest in free energy. The uncertainty in the OH* to O* phase transition in the range from ∼0.6 to ∼0.8 V (RHE) is consistent to that reported earlier.[6] We note that in cyclic voltammetry experiments Wang et al.,[44] Koper,[45] and Garcia-Araez et al.[46,47] attribute the reversible butterfly region between 0.6 and 0.85 V to OH*, which is also supported by Wakisaka et al.[5] in ex situ X-ray photoelectron spectroscopy experiments. In line with these findings, although at $U \approx 0.63$ V (RHE) predictions from our analysis (Figure 3b) have very close energetics, we note that the highest prediction confidence for OH* adsorption occurs at this potential, a key observation that is missed from the surface Pourbaix diagram in Figure 1. This emphasizes the usefulness of the defined quantity $c_{sp=i}(U)$ in more robustly assigning electrode potential regimes for the stability of a given surface state, when close energetics can be resolved between surface phases through experimental validation or higher-order DFT. At U_{RHE} > 0.63 V (RHE), O* surface adsorption coverage gradually increases to higher oxygen coverage and higher c-values for 1/4O* and 1/2O* until dissolution at a potential of 1.18 V. The 2/3O* surface phase is not stable at potentials below the dissolution potential (at pH = 0). Wakisaka et al.[5] have reported that OH* formation begins at *E* > 0.6 V, continuing to increase until 0.8 V, which is captured within uncertainty bounds of our predictions. Our findings of a monotonic increase in the oxygen coverage compare well with blank voltammetry[7] of Pt(111) in 0.1 M $HClO_4$, avoiding the specific adsorption of sulfate that occurs in sulfuric acid electrolyte. We believe that the correlation between our predictions and state-of-the-art experiments strengthens the effectiveness of confidence values and Bayesian error-estimation tools in quantifying uncertainty of predicted stability of surface phases.

3.2. Pt(100). We apply a similar methodology to Pt(100), which has been well studied both experimentally[48−50] and computationally[23,51] since commercial state-of-the-art Pt catalysts are comprised typically of low-index (111) and (100) facets.[52,53] We consider the following surface states of

DOI: 10.1021/acs.langmuir.8b02219
Langmuir 2018, 34, 12259−12269

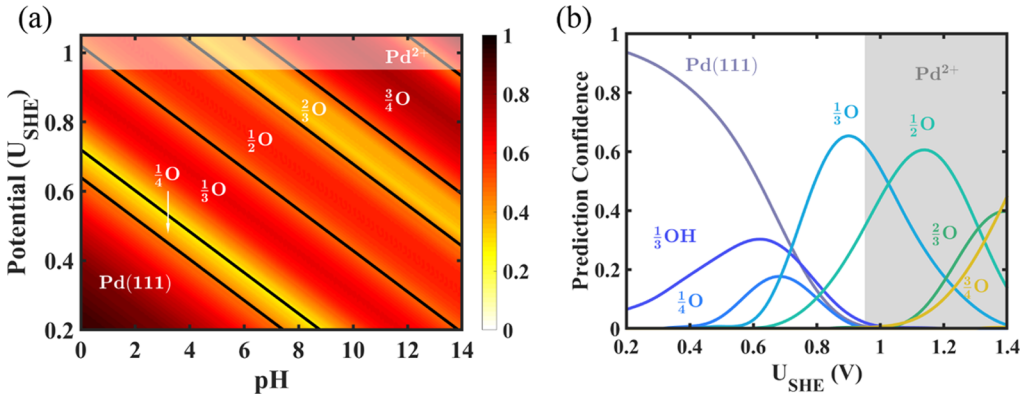

Figure 5. (a) Shows the surface Pourbaix diagram for Pd(111), where at pH = 0 oxidation is predicted to begin at 0.64 V (vs RHE). (b) Shows the c-value for each surface state at pH = 0, where transition to oxygen-covered surfaces begins at $U > 0.7$ V. The shaded gray region represents the onset of dissolution of crystalline Pd at 0.95 V.

Pt(100): 1/3OH*, 1/2OH*, 1/4O*, 1/2O*, 3/4O*, and 1O*. The surface phase boundaries in Figure 4a are determined using the best-fit BEEF−vdW functional. On the surface Pourbaix diagram, we overlay the c-values as a function of pH and potential, which provide a measure of agreement between GGA level functionals in the BEEF−vdW family of functional. We find that at $U_{RHE} < 0.64$ V, the clean Pt(100) surface is thermodynamically most favorable. At higher potentials, we predict 1/3OH* until 0.87 V (RHE) at which there is a narrow potential window where the 1/2OH* phase is the lowest in free energy. At $U_{RHE} \approx >0.9$ V, the OH* phase transitions to the 3/4O* surface. We observe that the prediction confidence (c-value) of the OH* surface states is relatively low (≈<0.4). The narrow region for stable 1/2OH* suggests that precise determination of the phase boundaries for this state is computationally challenging with the best-fit BEEF−vdW functional. We show the degree of agreement within the ensemble of functionals as to the most stable surface phase for each individual surfaces state in Figure 4b. We see that in the range 0.6 V < U_{RHE} < 0.7 V, 1/3OH* has a marginally greater c-value than 1/2OH*. However, at ≈0.8 V (RHE) the 1/2OH* surface state has a c-value of <0.25 suggesting that the 1/3OH* phase transitions to the more thermodynamically stable 1/2OH* with increasing electrode potential. Previously it was suggested through ab initio DFT calculations and Monte Carlo simulations[23] that 1/3OH* transforms into 1/2OH*, which is supported by our analysis; we find that 1/2OH* has the greatest confidence between 0.75 and 0.9 V (vs RHE). Of all oxygen-covered surfaces considered, at $U_{RHE} > 0.9$ V we predict the 3/4O* adsorption state to be the most favorable until the dissolution potential. On the basis of cyclic voltammetry in hydrochloric acid performed by several groups[49,50] a wide reversible peak centered at 0.36 V (vs RHE) has been reported and attributed to a strong overlap between hydrogen and OH* adsorption regions, which makes precise determination of adsorbed states difficult. Gómez et al.[50] used a deconvolution analysis to decouple OH coverage from H coverage, and in a subsequent work a maximum coverage value of 0.37 OH species per Pt surface atom was reported,[49] which corresponds to OH* adsorption assigned to a shoulder of the reversible peak appearing between 0.5 and 0.7 V on the cyclic voltammograms. We highlight that the prediction from our analysis for the clean Pt(100) surface transition to OH* (1/3OH* at 0.65 V vs RHE) falls within this region although the relatively low (<0.4) confidence values indicate the uncertainty associated with this transition. Similar to the case of Pt(111), this again emphasizes the efficacy of the defined quantity $c_{sp=i}(U)$ in assigning potential regimes for the stability of a given surface state, when close energetics can be resolved between surface phases through insights from both theory and experiments. We do not consider H* adsorption since it is beyond the scope of the current work owing to the necessary coverage-dependent analysis.[54]

3.3. Pd(111). Palladium has been identified to be a promising alternative to Pt for the ORR.[55−58] We construct the Pourbaix diagram for Pd(111) by considering the following states of the surface[59] similar to those considered for Pt(111): clean surface, 1/3OH*, 1/4O*, 1/3O*, 1/2O*, 2/3O*, 3/4O*, and 1O*. We predict from the constructed surface Pourbaix diagram, shown in Figure 5a, that the surface is clear of adsorbates until a potential of 0.64 V (vs RHE), which marks the onset of 1/4O* coverage surface state. At higher electrode potentials, O* adsorption increases monotonically to 1/3O* followed by 1/2O*, 2/3O*, and finally by 3/4O*. Pd $\rightleftharpoons$ Pd^{2+} + $2e^-$ dissolution is labeled at 0.95 V, which is independent of pH. Relatively low (<0.4) prediction confidence regions in Figure 5a show that transitions between 1/4O* and 1/3O* in particular have a high degree of uncertainty along with the 2/3O* surface state transitions between 1/2O* and 3/4O* regions, which we inspect further using $c_{sp=i}(U, \text{pH} = 0)$ (refer to Section 2.3) for all i corresponding to the considered surface phases. On the basis of this uncertainty quantification measure, for each surface phase we depict the agreement within the BEEF−vdW ensemble of functionals in Figure 5b. We notice a low degree of prediction confidence as to the lowest free-energy surface phase at ≈0.72 V (vs RHE) (pH = 0) where the maximum c-value is <0.3. The 1/3OH* surface has a relatively higher confidence value than the 1/4O* surface suggesting that the clean surface transitions directly to the 1/3OH* surface phase, an observation enabled by the defined quantity $c_{sp=i}(U, \text{pH})$. Experimentally, Hara et al.[24] ascribe broad anodic and cathodic current peaks to OH* species around 0.7 V based on cyclic voltammetry in perchloric acid solution. We quantify the maximum observed c-value for 1/3OH* between 0.6 and 0.7 V (vs RHE), which lies close to the experimentally observed region within the prediction uncertainty. We observe comparatively large prediction confidence values for 1/3O*- and 1/2O*-covered surfaces between 0.8 and 1.3 V (vs RHE),

DOI: 10.1021/acs.langmuir.8b02219
Langmuir 2018, 34, 12259−12269

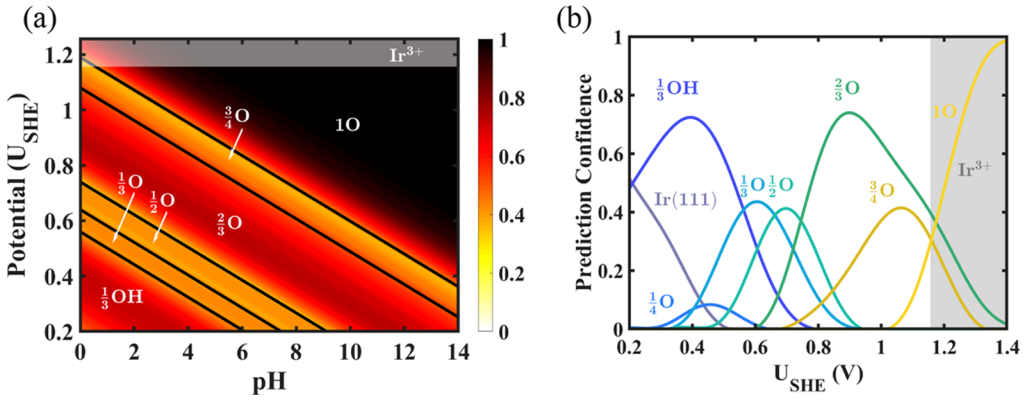

Figure 6. (a) Shows the surface Pourbaix diagram for Ir(111), where we observe oxidation to begin with 1/3OH* in the range from 0.2 to 0.55 V. We then see increase in oxidation until the dissolution potential at 1.16 V. (b) Shows each stable region assigned prediction confidence on the surface Pourbaix at pH = 0 where we see a region with low confidence between 0.55 and 0.7 V. In this region, the surface may be covered by 1/3OH*, 1/3O*, 1/2O*, or 2/3O*. The shaded gray region on the *x*-axis represents dissolution into Ir^{3+} at 1.16 V.

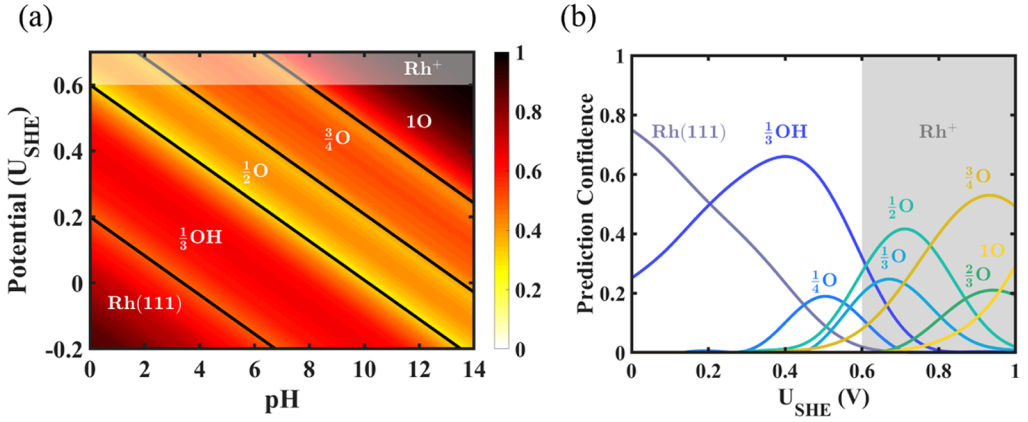

Figure 7. (a) Shows the surface Pourbaix diagram for Rh(111). (b) Describes the confidence for each surface state at pH = 0 where dissolution from solid Rh to Rh^{1+} is shown at 0.60 V by the shaded gray region.

which is supported by Hara et al., who report an oxidation peak corresponding to oxygen adsorption at 1.02 V.

3.4. Ir(111). Iridium is a highly corrosion-resistant platinum group metal and is similar to Pt although relatively less extensively studied.[60] Stable surface phases determined with the best-fit BEEF−vdW functional are shown with the bold black lines in the constructed surface Pourbaix diagram in Figure 6a. Oxygen coverage begins with 1/3OH* to potentials of ≈0.56 V (vs RHE) at pH = 0, consistent to prior DFT predictions that Ir is more oxophilic than Pt(111).[25,61] The surface transitions to 1/3O* at ≈0.56 V, followed by 1/2O* at ≈0.64 V, 2/3O* at ≈0.74 V, and 3/4O* at ≈1.1 V (all vs RHE), with dissolution at ≈1.16 V.[30] However, prediction confidence values corresponding to the 1/3O*, 1/2O*, and 3/4O* surface phases are low (c-value <0.4) relative to 1/3OH* phase. To further probe the degree of agreement within the ensemble of functionals as to the lowest free-energy phase especially close to the phase boundaries, we assess the uncertainty quantification metric $c_{sp=i}$ for all *i* corresponding to the considered surface phases, as shown in Figure 6b. We predict with high confidence the 1/3OH* adsorption phase approximately in the $0.2 < U < 0.55$ V (vs RHE) range where the c-value is >0.5 with a maximum at ≈0.4 V. We observe that between ≈0.55 and ≈0.75 V (vs RHE) a smooth transition from the 1/3O* phase to the 1/2O* phase. At higher potentials until dissolution, with a large degree of agreement between the functionals we predict the 2/3O* surface phase to be the lowest in free energy. The 3/4O* surface has a maximum c-value of nearly 0.4 at ≈1.0 V (vs RHE), therefore, within DFT uncertainty we expect a short voltage window where this phase is stable just before dissolution. We note some uncertainty concerning the interpretation of peaks in cyclic voltammograms while comparing the findings from our analysis. Cyclic voltammograms for Ir(111) in perchloric acid show a broad peak between approximately 0.05 and 0.35 V (vs RHE).[62−64] In this range, Koper suggests that the surface is covered with hydrogen, but also tentatively suggests that the peak could represent a mixed transition phase from being OH-covered to being H-covered,[45] whereas Wan et al. have attributed this region to hydrogen adsorption.[64] We find that our prediction of a stronger binding OH* surface as compared to Pt(111) is closer in agreement with previous DFT calculations.[25] Similarly, regarding the interpretation of a pair of sharp cyclic voltammetry peaks at 0.92 V and 0.95 V in perchloric acid, Wan et al.[64] attributes it to initial stages of oxidation representing hydroxide adsorption, but this would depend on the interpretation of the peak between 0.05 and 0.35 V since that would affect the length of the double-layer region.[45] With high confidence (c-value >0.7), we observe that the surface is O* covered at 0.9 V (vs RHE), which is in agreement with DFT calculations.[25] We highlight that the defined confidence values provide a way to incorporate DFT

DOI: 10.1021/acs.langmuir.8b02219
Langmuir 2018, 34, 12259−12269

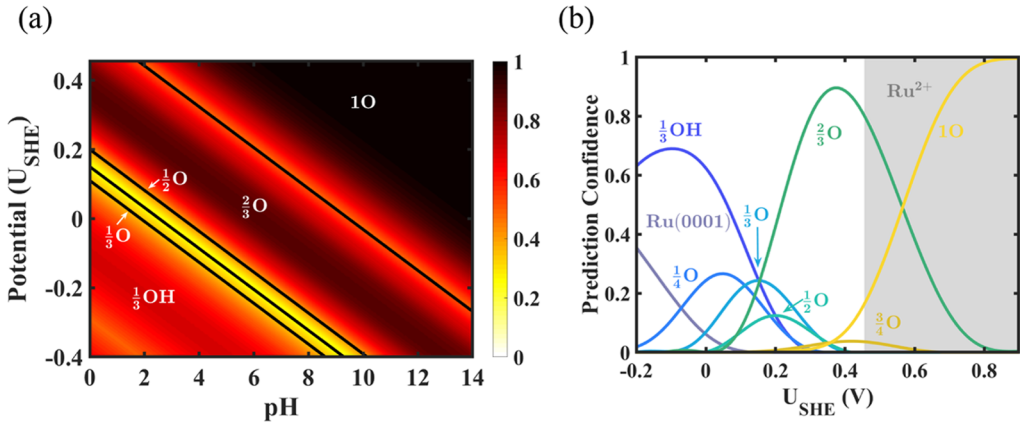

Figure 8. (a) Shows the surface Pourbaix diagram for Ru(0001) showing strong oxidation at low potentials. (b) Shows the confidence prediction for each surface state at pH of 0. The region on the *x*-axis shaded in gray shows the dissolution potential to Ru^{2+} occurring at 0.46 V.

uncertainty to interpret smooth surface phase transitions and aid a more integrated theory−experiment effort that is necessary for conclusive peak assignments.

3.5. Rh(111). The Pt-group metal rhodium is less frequently studied since it is scarce and expensive. However, it is a versatile catalyst most known for use in the three-way catalyst for NO_x reduction and oxidation of CO and unburned hydrocarbons in automotive exhaust.[65] We show the constructed surface Pourbaix diagram for the Rh(111) surface in Figure 7a. At pH = 0, we observe the 1/3OH* surface phase to be stable between ≈0.2 and 0.6 V (vs RHE). The surface Pourbaix diagram also shows that Rh(111) binds oxygen intermediates stronger than Pt(111), which is supported by prior DFT studies.[25,66] At pH = 0, we show that dissolution is favored at 0.6 V (vs RHE) of the crystalline Rh metal governed by the equilibrium relation $Rh^+ + e^- \rightleftharpoons Rh$. On the basis of the best-fit BEEF−vdW functional, at a constant electrode potential with increasing pH, we observe that the 1/2O* surface appears as the most stable phase followed by the 3/4O* phase and subsequently the 1O* surface phase. However, we notice that the 1/2O* phase is predicted to have a narrow stability region associated to a comparatively low (c-value < 0.4) degree of prediction confidence.

We understand the relative agreement between the functionals as to the lowest free-energy phase by constructing Figure 7b based on $c_{sp=i}(U, pH)$ for all *i* corresponding to the surfaces phases considered. We observe that 1/4O*, 1/3O*, and 2/3O* surface phases are associated with low confidence values (<0.3) in accordance with the fact that these phases do not appear in Figure 7a based on the best-fit BEEF−vdW functional. From Figure 7b at pH = 0, we predict the 1/3OH* surface to be stable between ≈0.2 and ≈0.6 V (vs RHE) with relatively high prediction confidence. Several experimental groups have studied cyclic voltammetry on Rh(111) in perchloric solutions to understand the sharp reversible peak visible at 0.64 V.[67−69] The reversible nature of this peak has led it to be tentatively ascribed to OH adsorption[45,67] although we predict the onset of 1/3OH* phase at a lower potential. However, we cautiously speculate that a surface reconstruction to RhO_2 occurs based on our prediction of the onset of OH* adsorption on RhO_2 at 0.66 V and the observed reversible butterfly peak at 0.64 V (refer to Section S4 of the Supporting Information for additional details). This reconstruction could correspond to the broad peak at ≈0.3 V and also explain why the dissolution potential for Rh to Rh^{1+} is experimentally observed[30] at 0.6 V, whereas the cyclic voltammogram extends until ≈0.8 V.[45,67] However, further insight into the stability of the Rh oxide through a surface Pourbaix diagram is necessary to validate the hypothesis.

3.6. Ru(0001). Ruthenium is used as a catalyst for nitrogen reduction[70,71] and is the basis for several bimetallic catalyst systems in electrocatalysts.[72,73] We consider the widely studied Ru(0001) surface for our analysis and consider oxygen adsorption at the hexagonal close-packed sites. The surface Pourbaix diagram for the hexagonal close-packed Ru(0001) surface is shown in Figure 8a with the narrow transition from 1/3OH* to 1/3O* surface configuration at 0.11 V (vs RHE) at a pH = 0, then at 0.15 V to 1/2O*, followed by transition at 0.2 V to 2/3O*. At a constant pH, with increasing potential, we observe a transition from the 2/3O* surface phase to the 1O* phase. Ru metal binds oxygen strongly with lower onset potentials for adsorption of oxygenated species relative to other transition metals, which is in agreement with a previous DFT study by Taylor et al.[43] From Figure 8a we calculate that the 1/3O* and 1/2O* surface states exhibit relatively low confidence (c-values < 0.3) resulting in high uncertainty spanning the OH* to O* transition. The 1/3OH* and 2/3O* surfaces in the Pourbaix diagram are predicted with a high level of confidence (≈ > 0.5).

We assess the relative prediction confidence of all surface phases using $c_{sp=i}$ by constructing Figure 8b at pH = 0. The maximum prediction confidence (c-value of 0.7) associated with the 1/3OH* phase occurs near −0.12 V (vs RHE). Our prediction of the OH* to O* phase transition at 0.16 V (vs RHE) is very close to that interpreted by Marc Koper[45] (0.18 V) from cyclic voltammetry[74−76] analysis on considering the DFT prediction error (σ_{OH} = 0.27, σ_O = 0.09). We note that experimentally confirmed 1/4O*,[77] 1/2O*,[78] 3/4O*,[79] and 1O*[80] surfaces have also been previously determined to be stable computationally along with the 2/3O* surface for a short window of stability.[81,82] We observe a much wider window of stability for 2/3O* than previously reported along with high degrees of prediction uncertainty (c-values < 0.3) for 1/4O*, 1/2O*, and 3/4O*, which we tentatively attribute to the tendency of the BEEF−vdW XC-functional to overbind oxygen.[26]

In Figure 8 the dissolution potential of crystalline Ru to Ru^{2+} under standard conditions is predicted at 0.46 V[30] but note that cyclic voltammograms in literature are cycled to >0.8 V suggesting surface reconstruction. Formation of Ru oxide,

DOI: 10.1021/acs.langmuir.8b02219
Langmuir 2018, 34, 12259−12269

particularly to $RuO_2(110)$, has been reported for Ru under high oxygen content both experimentally[83,84] and computationally.[85,86] This becomes critical to consider to analyze the surface Pourbaix diagram at higher potentials. We also note that consideration of a water layer on RuO_2 becomes more important in this case, as experiments by Krause et al.[87] have recently revealed the formation of hydrous RuO_2 under ultrahigh vacuum conditions, which would undoubtedly affect the interpretation between theory and experiment.

Further improvements to the uncertainty incorporation method presented here can be made by accounting for configurational and vibrational entropy and accounting for uncertainties in zero point energy although we expect these effects to be much smaller than the uncertainties accounted for in this paper. For increased prediction accuracy of surface reactivity of catalysts, systematically accounting for a self-consistent loop between the stable state of the surface determined by surface Pourbaix diagrams and the reactivity determined by the limiting potential derived from free-energy diagrams is essential. In addition, this work enables a precise determination of the stable catalyst surface state, which has important implications for identifying dominant reaction mechanisms and selectivity.

4. CONCLUSIONS

Surface Pourbaix diagrams are a crucial step in subsequent determination of electrocatalytic reaction mechanisms and in corrosion processes. In this work, we demonstrate a method to quantify uncertainty in density functional theory-calculated surface Pourbaix diagrams. Based on this method, we define a confidence value associated with each possible surface configuration at a given electrode potential, *U*, and pH. The approach involving the BEEF−vdW exchange correlation functional with built-in error-estimation capabilities is much more computationally efficient relative to performing many calculations based on different functionals since this involves non-self-consistent calculations based on the converged density from one self-consistent calculation. Using this method, we have constructed surface Pourbaix diagrams for each of Pt(111), Pt(100), Pd(111), Ir(111), Rh(111), and Ru(0001) surface and the associated confidence values for these surface phases. On Pt(111), our method captures the well-known uncertainty in the phase transition from OH* to O*. We find good agreement between our predicted phase diagrams on Pt(100) and Pd(111) compared to cyclic voltammetry experiments for the onset of OH* and O* covered surfaces. Ir(111), Rh(111), and Ru(0001) all exhibit strong oxidation of 1/3OH*, which supports prior theoretical studies. We also briefly consider oxidation on rutile metal oxides as a possible explanation to connect DFT and experimental observations. We suggest that reconstruction of the surface, particularly for Rh(111) and Ru(0001), could be important. An important implication from this work is the need to incorporate multiple surface phases in determining electrochemical reactions mechanisms and the associated activity due to finite uncertainty associated with predicting the stable state of the surface.

■ ASSOCIATED CONTENT

Supporting Information

The Supporting Information is available free of charge on the ACS Publications website at DOI: 10.1021/acs.langmuir.8b02219.

Calculation details; lattice parameters; calculating adsorption energies; adsorption on bulk oxide slabs; zero point and entropy corrections (PDF)

■ AUTHOR INFORMATION

Corresponding Author

*E-mail: venkvis@cmu.edu.

ORCID

Dilip Krishnamurthy: 0000-0001-8231-5492

Venkatasubramanian Viswanathan: 0000-0003-1060-5495

Notes

The authors declare no competing financial interest.

■ ACKNOWLEDGMENTS

O.V. gratefully acknowledges funding support in part from Volkswagen AG. D.K. and V.V. gratefully acknowledge funding support from the National Science Foundation under award CBET-1554273.

■ REFERENCES

(1) Lewis, N. S.; Nocera, D. G. Powering the planet: Chemical challenges in solar energy utilization. *Proc. Natl. Acad. Sci. U.S.A.* **2006**, *103*, 15729−15735.

(2) Montoya, J. H.; Seitz, L. C.; Chakthranont, P.; Vojvodic, A.; Jaramillo, T. F.; Nørskov, J. K. Materials for solar fuels and chemicals. *Nat. Mater.* **2017**, *16*, 70−81.

(3) Bockris, J. O.; Khan, S. U. *Surface Electrochemistry: A Molecular Level Approach*; Springer Science & Business Media, 2013.

(4) Bard, A. J.; Abruna, H. D.; Chidsey, C. E.; Faulkner, L. R.; Feldberg, S. W.; Itaya, K.; Majda, M.; Melroy, O.; Murray, R. W. The electrode/electrolyte interface-a status report. *J. Phys. Chem.* **1993**, *97*, 7147−7173.

(5) Wakisaka, M.; Suzuki, H.; Mitsui, S.; Uchida, H.; Watanabe, M. Identification and quantification of oxygen species adsorbed on Pt(111) single-crystal and polycrystalline Pt electrodes by photoelectron spectroscopy. *Langmuir* **2009**, *25*, 1897−1900.

(6) Casalongue, H. S.; Kaya, S.; Viswanathan, V.; Miller, D. J.; Friebel, D.; Hansen, H. A.; Nørskov, J. K.; Nilsson, A.; Ogasawara, H. Direct observation of the oxygenated species during oxygen reduction on a platinum fuel cell cathode. *Nat. Commun.* **2013**, *4*, No. 2817.

(7) Bondarenko, A. S.; Stephens, I. E.; Hansen, H. A.; Pérez-Alonso, F. J.; Tripkovic, V.; Johansson, T. P.; Rossmeisl, J.; Nørskov, J. K.; Chorkendorff, I. The Pt (111)/electrolyte interface under oxygen reduction reaction conditions: an electrochemical impedance spectroscopy study. *Langmuir* **2011**, *27*, 2058−2066.

(8) Hansen, H. A.; Rossmeisl, J.; Nørskov, J. K. Surface Pourbaix diagrams and oxygen reduction activity of Pt, Ag and Ni(111) surfaces studied by DFT. *Phys. Chem. Chem. Phys.* **2008**, *10*, 3722−3730.

(9) Rao, R. R.; Kolb, M. J.; Halck, N. B.; Pedersen, A. F.; Mehta, A.; You, H.; Stoerzinger, K. A.; Feng, Z.; Hansen, H. A.; Zhou, H.; et al. Towards identifying the active sites on RuO 2 (110) in catalyzing oxygen evolution. *Energy Environ. Sci.* **2017**, *10*, 2626−2637.

(10) Seh, Z. W.; Kibsgaard, J.; Dickens, C. F.; Chorkendorff, I.; Nørskov, J. K.; Jaramillo, T. F. Combining theory and experiment in electrocatalysis: Insights into materials design. *Science* **2017**, *355*, eaad4998.

(11) Pourbaix, M.; Van Muylder, J.; De Zoubov, N. Electrochemical properties of the platinum metals. *Platinum Met. Rev.* **1959**, *3*, 47−53.

(12) Sumaria, V.; Krishnamurthy, D.; Viswanathan, V. Quantifying Confidence in DFT Predicted Surface Pourbaix Diagrams and Associated Reaction Pathways for Chlorine Evolution. *ACS Catal.* **2018**, *8*, 9034−9042.

(13) Hansen, H. A.; Man, I. C.; Studt, F.; Abild-Pedersen, F.; Bligaard, T.; Rossmeisl, J. Electrochemical chlorine evolution at rutile oxide (110) surfaces. *Phys. Chem. Chem. Phys.* **2010**, *12*, 283−290.

DOI: 10.1021/acs.langmuir.8b02219
Langmuir 2018, 34, 12259−12269

(14) Exner, K. S.; Sohrabnejad-Eskan, I.; Anton, J.; Jacob, T.; Over, H. Full Free Energy Diagram of an Electrocatalytic Reaction over a Single-Crystalline Model Electrode. *ChemElectroChem* **2017**, *4*, 2902−2908.
(15) Exner, K. S.; Sohrabnejad-Eskan, I.; Over, H. A Universal Approach To Determine the Free Energy Diagram of an Electrocatalytic Reaction. *ACS Catal.* **2018**, *8*, 1864−1879.
(16) Exner, K. S. Constrained Ab Initio Thermodynamics: Transferring the Concept of Surface Pourbaix Diagrams in Electrocatalysis to Electrode Materials in Lithium-Ion Batteries. *ChemElectroChem* **2017**, *4*, 3231−3237.
(17) Exner, K. S. A short perspective of modeling electrode materials in lithium-ion batteries by the ab initio atomistic thermodynamics approach. *J. Solid State Electrochem.* **2018**, 1−7.
(18) Tian, F.; Jinnouchi, R.; Anderson, A. B. How potentials of zero charge and potentials for water oxidation to OH(ads) on Pt(111) electrodes vary with coverage. *J. Phys. Chem. C* **2009**, *113*, 17484−17492.
(19) Jinnouchi, R.; Anderson, A. B. Aqueous and surface redox potentials from self-consistently determined Gibbs energies. *J. Phys. Chem. C* **2008**, *112*, 8747−8750.
(20) Exner, K. S.; Anton, J.; Jacob, T.; Over, H. Controlling Selectivity in the Chlorine Evolution Reaction over RuO2-Based Catalysts. *Angew. Chem., Int. Ed.* **2014**, *53*, 11032−11035.
(21) Wellendorff, J.; Lundgaard, K. T.; Møgelhøj, A.; Petzold, V.; Landis, D. D.; Nørskov, J. K.; Bligaard, T.; Jacobsen, K. W. Density functionals for surface science: Exchange-correlation model development with Bayesian error estimation. *Phys. Rev. B* **2012**, *85*, No. 235149.
(22) Rossmeisl, J.; Nørskov, J. K.; Taylor, C. D.; Janik, M. J.; Neurock, M. Calculated phase diagrams for the electrochemical oxidation and reduction of water over Pt(111). *J. Phys. Chem. B* **2006**, *110*, 21833−21839.
(23) Han, B.; Viswanathan, V.; Pitsch, H. First-principles based analysis of the electrocatalytic activity of the unreconstructed Pt(100) surface for oxygen reduction reaction. *J. Phys. Chem. C* **2012**, *116*, 6174−6183.
(24) Hara, M.; Linke, U.; Wandlowski, T. Preparation and electrochemical characterization of palladium single crystal electrodes in 0.1 M H_2SO_4 and $HClO_4$: Part I. Low-index phases. *Electrochim. Acta* **2007**, *52*, 5733−5748.
(25) Karlberg, G. Adsorption trends for water, hydroxyl, oxygen, and hydrogen on transition-metal and platinum-skin surfaces. *Phys. Rev. B* **2006**, *74*, No. 153414.
(26) Deshpande, S.; Kitchin, J. R.; Viswanathan, V. Quantifying Uncertainty in Activity Volcano Relationships for Oxygen Reduction Reaction. *ACS Catal.* **2016**, *6*, 5251−5259.
(27) Krishnamurthy, D.; Sumaria, V.; Viswanathan, V. Maximal predictability approach for identifying the right descriptors for electrocatalytic reactions. *J. Phys. Chem. Lett.* **2018**, *9*, 588−595.
(28) Exner, K. S.; Anton, J.; Jacob, T.; Over, H. Chlorine evolution reaction on RuO2 (110): Ab initio atomistic thermodynamics study-Pourbaix diagrams. *Electrochim. Acta* **2014**, *120*, 460−466.
(29) Exner, K. S.; Over, H. Kinetics of Electrocatalytic Reactions from First-Principles: A Critical Comparison with the Ab Initio Thermodynamics Approach. *Acc. Chem. Res.* **2017**, *50*, 1240−1247.
(30) Lide, D. R.; Kehiaian, H. V. *CRC Handbook of Thermophysical and Thermochemical Data*; CRC Press, 1994; Vol. *1*.
(31) Perdew, J. P.; Burke, K.; Ernzerhof, M. Generalized gradient approximation made simple. *Phys. Rev. Lett.* **1996**, *77*, 3865−3868.
(32) Lee, K.; Murray, É. D.; Kong, L.; Lundqvist, B. I.; Langreth, D. C. Higher-accuracy van der Waals density functional. *Phys. Rev. B* **2010**, *82*, No. 081101(R).
(33) Houchins, G.; Viswanathan, V. Quantifying confidence in density functional theory predictions of magnetic ground states. *Phys. Rev. B* **2017**, *96*, No. 134426.
(34) Garcia-Araez, N.; Climent, V.; Feliu, J. Potential-dependent water orientation on Pt(111), Pt(100), and Pt(110), as inferred from laser-pulsed experiments. Electrostatic and chemical effects. *J. Phys. Chem. C* **2009**, *113*, 9290−9304.
(35) Ogasawara, H.; Brena, B.; Nordlund, D.; Nyberg, M.; Pelmenschikov, A.; Pettersson, L.; Nilsson, A. Structure and bonding of water on Pt (111). *Phys. Rev. Lett.* **2002**, *89*, No. 276102.
(36) Stamenkovic, V. R.; Fowler, B.; Mun, B. S.; Wang, G.; Ross, P. N.; Lucas, C. A.; Marković, N. M. Improved oxygen reduction activity on Pt3Ni (111) via increased surface site availability. *Science* **2007**, *315*, 493−497.
(37) Greeley, J.; Stephens, I.; Bondarenko, A.; Johansson, T. P.; Hansen, H. A.; Jaramillo, T.; Rossmeisl, J.; Chorkendorff, I.; Nørskov, J. K. Alloys of platinum and early transition metals as oxygen reduction electrocatalysts. *Nat. Chem.* **2009**, *1*, 552−556.
(38) Viswanathan, V.; Hansen, H. A.; Rossmeisl, J.; Jaramillo, T. F.; Pitsch, H.; Nørskov, J. K. Simulating linear sweep voltammetry from first-principles: application to electrochemical oxidation of water on Pt(111) and Pt3Ni(111). *J. Phys. Chem. C* **2012**, *116*, 4698−4704.
(39) Liu, S.; White, M. G.; Liu, P. Mechanism of oxygen reduction reaction on Pt (111) in alkaline solution: Importance of chemisorbed water on surface. *J. Phys. Chem. C* **2016**, *120*, 15288−15298.
(40) Rossmeisl, J.; Karlberg, G. S.; Jaramillo, T.; Nørskov, J. K. Steady state oxygen reduction and cyclic voltammetry. *Faraday Discuss.* **2009**, *140*, 337−346.
(41) Stephens, I. E.; Bondarenko, A. S.; Grønbjerg, U.; Rossmeisl, J.; Chorkendorff, I. Understanding the electrocatalysis of oxygen reduction on platinum and its alloys. *Energy Environ. Sci.* **2012**, *5*, 6744−6762.
(42) Darling, R. M.; Meyers, J. P. Kinetic model of platinum dissolution in PEMFCs. *J. Electrochem. Soc.* **2003**, *150*, A1523−A1527.
(43) Taylor, C. D.; Kelly, R. G.; Neurock, M. First-principles prediction of equilibrium potentials for water activation by a series of metals. *J. Electrochem. Soc.* **2007**, *154*, F217−F221.
(44) Wang, J.; Markovic, N.; Adzic, R.; et al. Kinetic analysis of oxygen reduction on Pt(111) in acid solutions: intrinsic kinetic parameters and anion adsorption effects. *J. Phys. Chem. B* **2004**, *108*, 4127−4133.
(45) Koper, M. Blank voltammetry of hexagonal surfaces of Pt-group metal electrodes: comparison to density functional theory calculations and ultra-high vacuum experiments on water dissociation. *Electrochim. Acta* **2011**, *56*, 10645−10651.
(46) Garcia-Araez, N.; Climent, V.; Feliu, J. M. Determination of the entropy of formation of the Pt(111) perchloric acid solution interface. Estimation of the entropy of adsorbed hydrogen and OH species. *J. Solid State Electrochem.* **2008**, *12*, 387−398.
(47) Garcia-Araez, N.; Climent, V.; Herrero, E.; Feliu, J. M.; Lipkowski, J. Thermodynamic approach to the double layer capacity of a Pt(111) electrode in perchloric acid solutions. *Electrochim. Acta* **2006**, *51*, 3787−3793.
(48) Stamenkovic, V.; Markovic, N.; Ross, P., Jr Structure-relationships in electrocatalysis: oxygen reduction and hydrogen oxidation reactions on Pt(111) and Pt(100) in solutions containing chloride ions. *J. Electroanal. Chem.* **2001**, *500*, 44−51.
(49) Climent, V.; Gómez, R.; Orts, J. M.; Feliu, J. M. Thermodynamic analysis of the temperature dependence of OH adsorption on Pt(111) and Pt(100) electrodes in acidic media in the absence of specific anion adsorption. *J. Phys. Chem. B* **2006**, *110*, 11344−11351.
(50) Gómez, R.; Orts, J. M.; Álvarez-Ruiz, B.; Feliu, J. M. Effect of temperature on hydrogen adsorption on Pt(111), Pt(110), and Pt(100) electrodes in 0.1 M $HClO_4$. *J. Phys. Chem. B* **2004**, *108*, 228−238.
(51) Duan, Z.; Wang, G. Comparison of reaction energetics for oxygen reduction reactions on Pt(100), Pt(111), Pt/Ni(100), and Pt/Ni(111) surfaces: a first-principles study. *J. Phys. Chem. C* **2013**, *117*, 6284−6292.
(52) Song, H.; Kim, F.; Connor, S.; Somorjai, G. A.; Yang, P. Pt nanocrystals: shape control and langmuir- blodgett monolayer formation. *J. Phys. Chem. B* **2005**, *109*, 188−193.

DOI: 10.1021/acs.langmuir.8b02219
Langmuir 2018, 34, 12259−12269

(53) Wang, C.; Daimon, H.; Onodera, T.; Koda, T.; Sun, S. A General Approach to the Size-and Shape-Controlled Synthesis of Platinum Nanoparticles and Their Catalytic Reduction of Oxygen. *Angew. Chem., Int. Ed.* **2008**, *47*, 3588−3591.
(54) Karlberg, G. S.; Jaramillo, T.; Skulason, E.; Rossmeisl, J.; Bligaard, T.; Nørskov, J. K. Cyclic voltammograms for H on Pt(111) and Pt(100) from first principles. *Phys. Rev. Lett.* **2007**, *99*, No. 126101.
(55) Shao, M.-H.; Sasaki, K.; Adzic, R. R. Pd- Fe nanoparticles as electrocatalysts for oxygen reduction. *J. Am. Chem. Soc.* **2006**, *128*, 3526−3527.
(56) Fernández, J. L.; Raghuveer, V.; Manthiram, A.; Bard, A. J. Pd-Ti and Pd- Co- Au electrocatalysts as a replacement for platinum for oxygen reduction in proton exchange membrane fuel cells. *J. Am. Chem. Soc.* **2005**, *127*, 13100−13101.
(57) Fernández, J. L.; Walsh, D. A.; Bard, A. J. Thermodynamic guidelines for the design of bimetallic catalysts for oxygen electroreduction and rapid screening by scanning electrochemical microscopy. M- Co (M: Pd, Ag, Au). *J. Am. Chem. Soc.* **2005**, *127*, 357−365.
(58) Savadogo, O.; Lee, K.; Oishi, K.; Mitsushima, S.; Kamiya, N.; Ota, K.-I. New palladium alloys catalyst for the oxygen reduction reaction in an acid medium. *Electrochem. Commun.* **2004**, *6*, 105−109.
(59) Mitsui, T.; Rose, M.; Fomin, E.; Ogletree, D. F.; Salmeron, M. Water diffusion and clustering on Pd(111). *Science* **2002**, *297*, 1850−1852.
(60) Cherevko, S.; Geiger, S.; Kasian, O.; Kulyk, N.; Grote, J.-P.; Savan, A.; Shrestha, B. R.; Merzlikin, S.; Breitbach, B.; Ludwig, A.; et al. Oxygen and hydrogen evolution reactions on Ru, RuO_2, Ir, and IrO_2 thin film electrodes in acidic and alkaline electrolytes: a comparative study on activity and stability. *Catal. Today* **2016**, *262*, 170−180.
(61) Krekelberg, W. P.; Greeley, J.; Mavrikakis, M. Atomic and molecular adsorption on Ir(111). *J. Phys. Chem. B* **2004**, *108*, 987−994.
(62) Ganassin, A.; Sebastián, P.; Climent, V.; Schuhmann, W.; Bandarenka, A. S.; Feliu, J. On the pH Dependence of the Potential of Maximum Entropy of Ir (111) Electrodes. *Sci. Rep.* **2017**, *7*, No. 1246.
(63) Pajkossy, T.; Kibler, L.; Kolb, D. Voltammetry and impedance measurements of Ir (111) electrodes in aqueous solutions. *J. Electroanal. Chem.* **2005**, *582*, 69−75.
(64) Wan, L.-J.; Hara, M.; Inukai, J.; Itaya, K.; et al. In situ scanning tunneling microscopy of well-defined Ir(111) surface: high-resolution imaging of adsorbed sulfate. *J. Phys. Chem. B* **1999**, *103*, 6978−6983.
(65) Heck, R. M.; Farrauto, R. J. Automobile exhaust catalysts. *Appl. Catal., A* **2001**, *221*, 443−457.
(66) Marković, N.; Ross, P. N. Surface science studies of model fuel cell electrocatalysts. *Surf. Sci. Rep.* **2002**, *45*, 117−229.
(67) Housmans, T.; Koper, M. CO oxidation on stepped Rh [*n*(1 1 1) × (1 1 1)] single crystal electrodes: Anion effects on CO surface mobility. *Electrochem. Commun.* **2005**, *7*, 581−588.
(68) Clavilier, J.; Wasberg, M.; Petit, M.; Klein, L. Detailed analysis of the voltammetry of Rh(111) in perchloric acid solution. *J. Electroanal. Chem.* **1994**, *374*, 123−131.
(69) Wan, L.-J.; Yau, S.-L.; Swain, G. M.; Itaya, K. In-situ scanning tunneling microscopy of well-ordered Rh(111) electrodes. *J. Electroanal. Chem.* **1995**, *381*, 105−111.
(70) Jacobsen, C. J.; Dahl, S.; Hansen, P. L.; Törnqvist, E.; Jensen, L.; Topsøe, H.; Prip, D. V.; Møenshaug, P. B.; Chorkendorff, I. Structure sensitivity of supported ruthenium catalysts for ammonia synthesis. *J. Mol. Catal. A: Chem.* **2000**, *163*, 19−26.
(71) Aika, K.-i.; Hori, H.; Ozaki, A. Activation of nitrogen by alkali metal promoted transition metal I. Ammonia synthesis over ruthenium promoted by alkali metal. *J. Catal.* **1972**, *27*, 424−431.
(72) Hansen, T. W.; Hansen, P. L.; Dahl, S.; Jacobsen, C. J. Support effect and active sites on promoted ruthenium catalysts for ammonia synthesis. *Catal. Lett.* **2002**, *84*, 7−12.
(73) Jackson, A.; Viswanathan, V.; Forman, A. J.; Larsen, A. H.; Nørskov, J. K.; Jaramillo, T. F. Climbing the activity volcano: core−shell Ru at Pt electrocatalysts for oxygen reduction. *ChemElectroChem* **2014**, *1*, 67−71.
(74) Zhou, W.-P.; Lewera, A.; Bagus, P. S.; Wieckowski, A. Electrochemical and electronic properties of platinum deposits on Ru(0001): Combined XPS and cyclic voltammetric study. *J. Phys. Chem. C* **2007**, *111*, 13490−13496.
(75) Hoster, H.; Richter, B.; Behm, R. Catalytic influence of Pt monolayer islands on the hydrogen electrochemistry of Ru(0001) studied by ultrahigh vacuum scanning tunneling microscopy and cyclic voltammetry. *J. Phys. Chem. B* **2004**, *108*, 14780−14788.
(76) El-Aziz, A.; Kibler, L. New information about the electrochemical behaviour of Ru(0001) in perchloric acid solutions. *Electrochem. Commun.* **2002**, *4*, 866−870.
(77) Lindroos, M.; Pfnür, H.; Held, G.; Menzel, D. Adsorbate induced reconstruction by strong chemisorption: Ru (001) p (2 × 2)-O. *Surf. Sci.* **1989**, *222*, 451−463.
(78) Pfnür, H.; Held, G.; Lindroos, M.; Menzel, D. Oxygen induced reconstruction of a close-packed surface: a LEED IV study on Ru (001)-p (2 × 1) O. *Surf. Sci.* **1989**, *220*, 43−58.
(79) Kim, Y.; Wendt, S.; Schwegmann, S.; Over, H.; Ertl, G. Structural analyses of the pure and cesiated Ru (0001)-(2 × 2)-3O phase. *Surf. Sci.* **1998**, *418*, 267−272.
(80) Stampfl, C.; Schwegmann, S.; Over, H.; Scheffler, M.; Ertl, G. Structure and stability of a high-coverage (1 × 1) oxygen phase on Ru (0001). *Phys. Rev. Lett.* **1996**, *77*, 3371−3374.
(81) Stampfl, C. Surface processes and phase transitions from ab initio atomistic thermodynamics and statistical mechanics. *Catal. Today* **2005**, *105*, 17−35.
(82) Stampfl, C.; Soon, A.; Piccinin, S.; Shi, H.; Zhang, H. Bridging the temperature and pressure gaps: close-packed transition metal surfaces in an oxygen environment. *J. Phys.: Condens. Matter* **2008**, *20*, No. 184021.
(83) Lin, W.; Zei, M.; Kim, Y.; Over, H.; Ertl, G. Electrochemical versus gas-phase oxidation of Ru single-crystal surfaces. *J. Phys. Chem. B* **2000**, *104*, 6040−6048.
(84) Over, H.; Kim, Y. D.; Seitsonen, A.; Wendt, S.; Lundgren, E.; Schmid, M.; Varga, P.; Morgante, A.; Ertl, G. Atomic-scale structure and catalytic reactivity of the RuO2 (110) surface. *Science* **2000**, *287*, 1474−1476.
(85) Reuter, K.; Stampfl, C.; Ganduglia-Pirovano, M. V.; Scheffler, M. Atomistic description of oxide formation on metal surfaces: the example of ruthenium. *Chem. Phys. Lett.* **2002**, *352*, 311−317.
(86) Reuter, K.; Ganduglia-Pirovano, M. V.; Stampfl, C.; Scheffler, M. Metastable precursors during the oxidation of the Ru (0001) surface. *Phys. Rev. B* **2002**, *65*, No. 165403.
(87) Krause, P. P.; Camuka, H.; Leichtweiss, T.; Over, H. Temperature-induced transformation of electrochemically formed hydrous RuO 2 layers over Ru (0001) model electrodes. *Nanoscale* **2016**, *8*, 13944−13953.

DOI: 10.1021/acs.langmuir.8b02219
Langmuir 2018, 34, 12259−12269